CAVITATION BUBBLE BEHAVIOR NEAR SOLID BOUNDARIES

H. Ishida, C. Nuntadusit and H. Kimoto
Graduate School of Engineering Science, Osaka University
Toyonaka, Osaka 560-8531, Japan

T. Nakagawa
Matsushita Electric Industry, Kadoma, Osaka 571-8501, Japan

T. Yamamoto
Daikin Industry, Kita-ku, Osaka 530-8323, Japan

Abstract

In the present study the bubble behavior in the narrow space are experimentally and numerically examined as the gap between two parallel walls and the position of bubble induction were changed. The main results are as follows. (1) The effects of two parallel walls can be classified by the ratio of the gap between the walls to the maximum bubble radius. If the ratio>5.0 the bubble shape is almost sphere. The wall effect remarkably appears for the ratio<3.0 and the bubble deforms to be dumbbell- or cone-like shape. (2) When the gap between the walls is small, the single bubble is finally divided into two bubbles owing to the large lateral pressure. The rebound of each bubble causes impulsive pressure and damages the upper and lower wall surface. Especially, if the bubble is not created at the center between the walls, the collapse phase shift among the divided bubbles brings the further damage on the wall surface. (3) The computed motion of the bubble without non-condensable gases well explains the dumbbell- or cone-shaped bubble deformation.

1 Introduction

Cavitation damage to solid surface is a major concern on the design of turbo-machinery and there have been many investigations on the bubble behavior or bubble dynamics near solid boundaries (Brennen 1995).

Lauterborn & Bolle (1975) examined the dynamics of bubbles near a solid boundary by high-speed photography and they were able to observe the variation of bubble shape and measure the tip velocity at bubble collapse. Tomita & Shima (1990) carried out precise experiments on the bubble behavior near a solid boundary as the distance from the bubble to the wall surface and the wall shape were changed, and found that the formation of disk-shaped bubble followed by the penetration of liquid jet on the concave wall surface may generate extreme high pressure by the shock focussing. There have been many discussions on the issue of which of microjets and shock waves cause the cavitation damage and, in this connection, Kimoto (1987) observed stress pulses that is caused by both microjet impingement and the remnant cloud collapse shock and showed that, typically, the impulsive pressures from the latter are 2 to 3 times larger than those from the microjet.

Moreover, there have been many numerical investigations on above-mentioned bubble dynamics. Plesset & Chapman (1971) numerically examined the change of bubble shapes near a solid wall and evaluated the velocity of microjet. The computed bubble motion and velocity of microjet are in good agreement with the experimental results of Lauterborn & Bolle (1975). More accurate computation (Blake et al. 1986) was performed using the boundary element method (BEM) and showed that there should be the 'optimal' condition at which the damage to the solid boundary becomes maximum. Best & Kucera (1992) precisely examined the motion of bubbles with non-condensable gas and found that the presence of non-condensable bubble contents can arrest jet formation. Furthermore, Best (1993) performed the simulation on the formation of toroidal bubbles and clarified the oscillatory nature of the bubbles. Takahira et al. (1997) also carried out the numerical study on the toroidal bubble and showed that the pressure on the concave wall induced by the bubble collapse is higher than that on the convex wall. This result supports the deduction of Tomita and Shima (1990).

On the other hand, there are few investigations on the bubble behavior between two solid parallel walls. Chahine (1982) experimentally examined such bubble behavior in the test solution with and without drag-reducing polymer and showed that the presence of the polymer shorten the bubble's lifetime. Moreover Kucherenko & Shamko (1986) also experimentally examined the bubbles between two solid parallel walls and observed the formation of dumbbell- or cone-shaped bubble when the gap between two parallel walls is shortened. When the gap is sufficiently large,

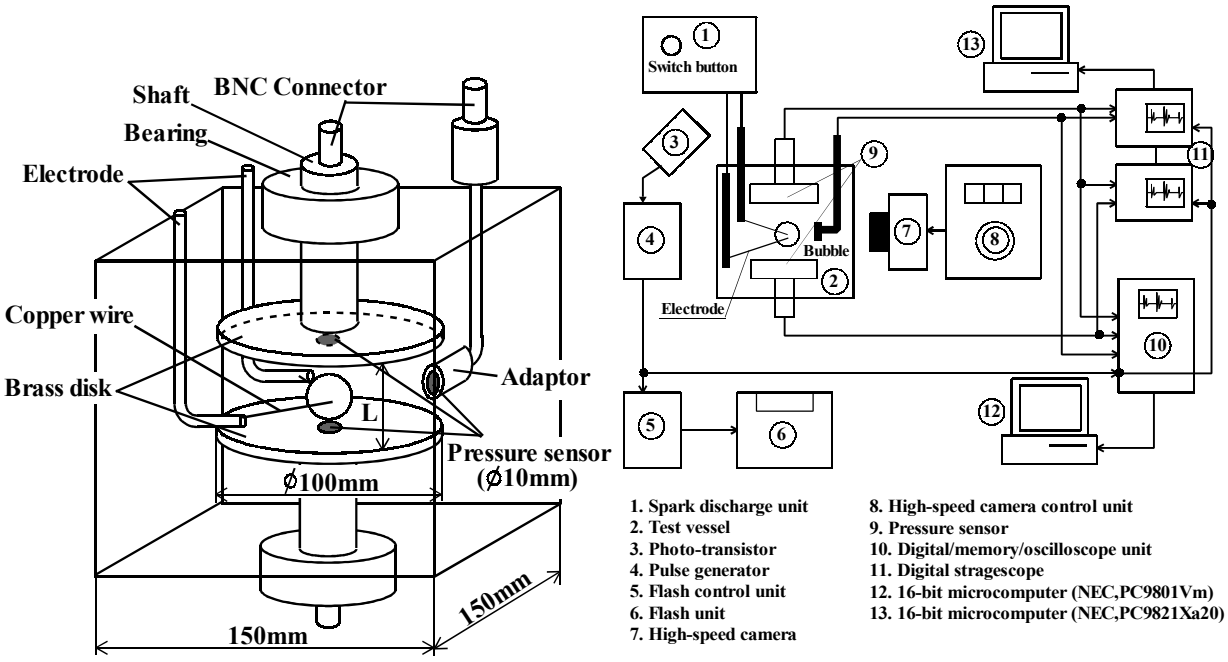

Figure 1: Left: test section. Right: schematic diagram of experimental setup

some analytical or numerical results based on asymptotic theory (Shima & Sato 1977; Chahine 1982) partly explain the above-mentioned behavior of bubbles. However these approach cannot be applied to the bubble motion in the narrow space.

In the present study the cavitation behavior between two parallel walls were experimentally and numerically examined. Firstly, changing the gap between the walls and the position of bubble formation, the variation of bubble shape was photographed using high-speed camera. Simultaneously the impulsive pressure change at some points was also measured by pressure sensors. Next, some numerical analyses based on BEM, that is applicable to the bubble dynamics in the narrow space, were carried out and the computed bubble motion was compared with the experimental one.

2 Experiment

2.1 Experimental Equipment and Method

In the present study a single bubble was induced by the electrical discharge between two flat plates in sufficiently boiled and then cooled water. The test section and the water tank is shown in figure 1. The inner size of the water tank is 150 mm long, 150 mm wide and 145 mm high and this tank is made of acrylic resin plates 10 mm thick. The flat plates in the tank consist of two parallel brass disks of 100 mm diameter combined with a movable shaft and the distance between the plates L can be changed between 0mm and 80 mm. Two copper wires of 0.3 mm diameter were inserted between the plates and used as electrodes, and the electrical discharge between them induce a bubble of nearly 14 mm diameter. In the present study the point of the electric discharge is on the joint center axis of the two disks. The experiment was performed under atmospheric one and the local change from the static pressure was measured by three pressure sensors of 10 mm diameter and 2.7 mm depth. Two of them were embedded on the center surface of each parallel disk and the remainder was fixed at the point of the same height as the electric-discharge point, 51 mm apart from the center axis of the disks, and turns its pressure-detecting face to the induced bubble. The third sensor was fixed by the adapter combined with a movable copper-pipe shaft.

As shown in figure 1 the sensors' electromotive force was measured by a digital memory/oscilloscope unit for 5 ms at intervals of 5 μs via BNC cable and simultaneously the same force was measured by two digital stragescopes for 1 ms at intervals of 0.5 μs with the delay time of 1 ms. Their voltage data were separately transmitted to microcomputers and recorded there for the following analyses. For synchronization the light emission by the electric discharge was detected by a photo-transistor and its output signal was used as the trigger to start a pulse generator. The generated rectangular electric pulse was fed into a flush control unit and light a flush for 4 ms, and the bubble

behavior was photographed by the open-shuttered high-speed movie camera at the framing rate of 41000 flames/s. This camera has the maximum framing number of 200 frames. The generated pulse mentioned above was also used as the trigger signal of data sampling by the digital oscilloscope unit and the digital stragescopes.

In the present experiment the bubble behavior and the pressure change were examined as the gap between two parallel plates L and the position of bubble induction h from the lower plate were changed. As preliminary experiment, the bubble behavior and the pressure change were examined for the case of L=80 mm and h=40 mm. The resultant bubble shape is almost spherical and its motion is qualitatively related to the behavior described by the Rayleigh-Plesset equation. The maximum radius of bubble was 8.3 mm. This indicates that the effects of wall are small in this case. The pressure sensor detect the impulsive pressure at the bubble rebound and its local maximum was used as the reference pressure P_r in the following discussion.

Next, the distance between the two plates L is shortened from 36 mm to 15 mm with the electric-discharge point fixed at the center between two parallel wall, i.e. h=L/2. The experiment for the case of L=15 mm and h=9 mm was also carried out.

2.2 Results and Discussion

For the case of L>15 mm the effects of two parallel walls are relatively small and the corresponding bubble has spherical (L=36 mm) or vertically-long spheroidal shape (L=25, 18 mm). Therefore we confine the following discussion to the case of L=15 mm.

In the following the dimensional variable Q is normalized by the representative length R_r, the representative velocity V_r and the above-mentioned representative pressure P_r. And the normalized quantity is described as Q^*. Herein V_r is defined as follows:

$$V_r \equiv \sqrt{\Delta P / \rho}\ , \quad \Delta P \equiv P_\infty - P_s\ , \tag{1}$$

where

P_∞ : atmospheric pressure, P_s : saturated vapor pressure.

In the present study the representative length R_r is defined as the equivalent radius of sphere R_m whose volume is the same as the maximum volume of the unsteadily deforming bubble.

The sample photographs for the case of L=15 mm and h=7.5 mm are shown in figure 2. The frame number, which is counted from the starting photograph of the light emission by the electrical discharge, is also described under each photograph. In this case the equivalent maximum radius of bubble R_m was 6.94 mm. Therefore the normalized quantities L^* and h^* are evaluated 2.16 and 1.08, respectively. Following the notation of the previous studies (Blake 1986; Best 1992) h^* is hereafter referenced as γ. The normalized time t^* is also put in the parentheses under the corresponding photograph.

In the expanding process the bubble maintains its spherical shape and reaches the volumetrical maximum at t^*=1.09. Since then the bubble laterally shrinks to be 'dumbbell-type' at t*=2.39, which is indicated by Kucherenko 1986, with its longitudinal length almost fixed. After that the upper and lower bubble are completely separated (t^*=2.43) and each bubble shrinks and rebounds at t^*=2.50. The rebounded bubble thereafter rebounds again around t^*=3.80 through expansion and collapse phase.

Above-mentioned bubble behavior can be ascertained on the output of pressure transducers. The normalized pressure change measured by the digital oscilloscope is shown in figure 3. The subscript 'st' denotes static pressure. In this figure the pressure fluctuation for t*< 1.44 is the noise due to the electrical discharge. The impulsive pressure is detected in the upper and lower wall sensors at t*=2.5 and corresponds well with the first rebound of the separated bubbles. The corresponding impulsive pressure is also detected in the pressure sensor outside the region between the two disks when the delay time is evaluated 30 μs (=0.04 dimensionless time) from the sound velocity 1500 m/s. Not shown in these figures, the small peak of about 0.1 is detected in the outer sensor at t^*=2.45 by the digital stragescope and this corresponds well with the attachment of lateral bubble wall followed by the bubble separation to the upper and lower sides. This local peak is not detected in the wall sensors. This is due to the presence of the upper and lower bubbles to prevent the propagation of the shock wave caused by the lateral wall attachment.

Next, the sample photographs for the case of L=15 mm and h=9 mm are also shown in figure 4. In this case the equivalent maximum radius of deforming bubble Rm=6.73 mm and, therefore, L^* and γ become 2.23 and 1.34, respectively.

In this case the induced bubble has the spherical shape in the early stage and after that the top of the bubble is gradually flattened out along the upper plate. The fully expanded bubble (t*=1.12) has the spheroidal shape with its top truncated by a horizontal plane, and then the practical bubble center is at the position of h=8.6 mm, i.e. γ=1.28.

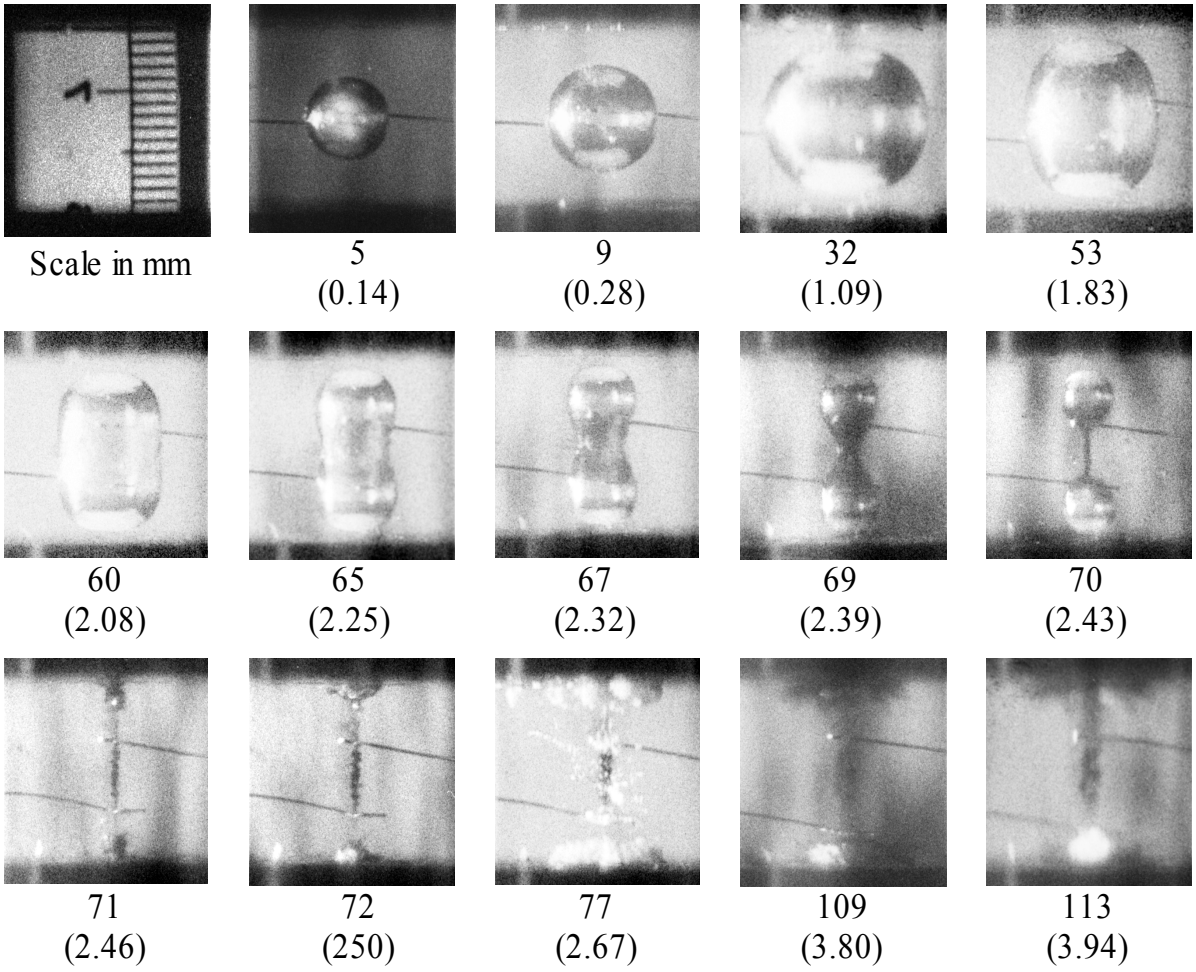

Figure 2: Electric-induced bubble behavior characterized by L=15 mm and h=7.5 mm. The framing rate is 41000 frame/s. The equivalent maximum bubble radius R_m=6.93 mm. The corresponding frame number and normalized time are also described under each photograph.

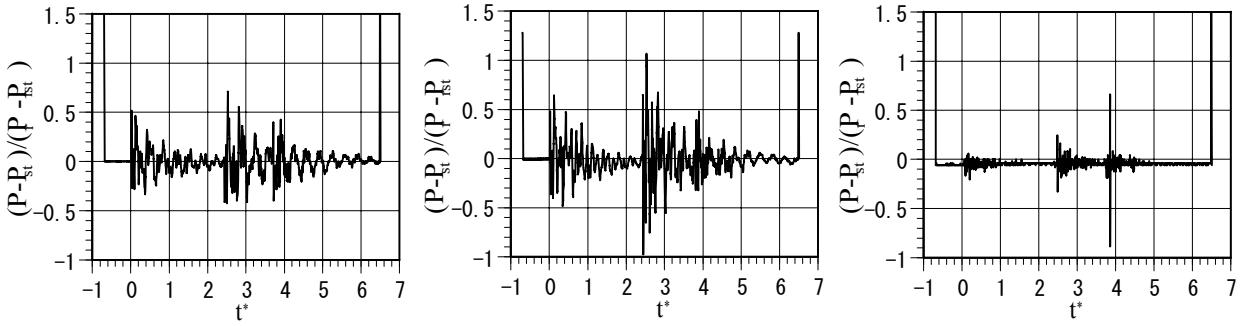

Figure 3: The normalized output of the pressure sensor for the case of L=15 mm and h=7.5 mm. Left: sensor output on the upper wall surface. Center: sensor output on the lower wall surface. Right: outer sensor output 51 mm apart from the joint center axis of the two parallel disks.

This bubble descent of 0.4 mm is due to the bubble-wall interaction. Afterward lateral shrink is observed as the previous case and the bubble becomes to be 'cone-like' shape at t^*=2.39, which is also indicated by Kucherenko 1986, and the bubble separates into upper and lower bubbles. The latter rebounds at t*=2.43 and the former rebounds at t^*=2.54 and 3.62. Moreover the remaining long and narrow bubble at the center between the walls also rebounds at t*=2.75.

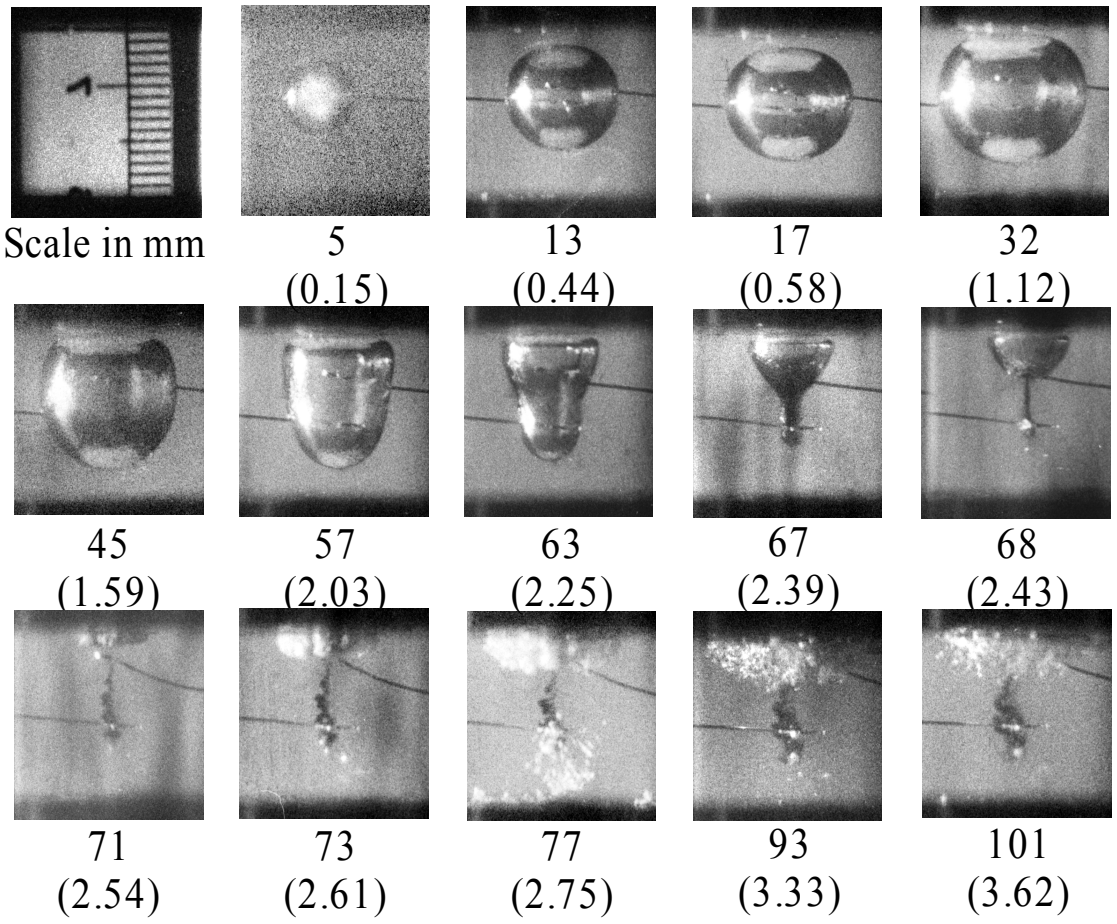

Figure 4: Electric-induced bubble behavior characterized by L=15 mm and h=9 mm. The framing rate is 41000 frame/s. The equivalent maximum bubble radius R_m=6.73 mm.

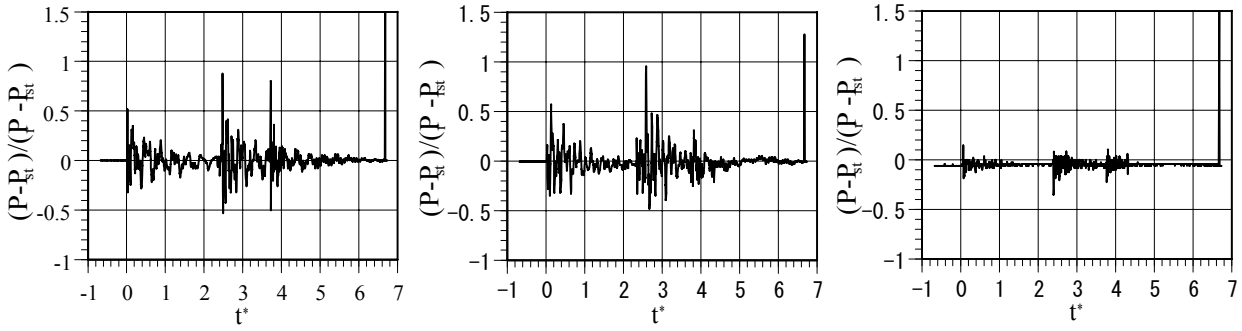

Figure 5: The normalized output of the pressure sensor for the case of L=15 mm and h=9 mm. Left: sensor output on the upper wall surface. Center: sensor output on the lower wall surface. Right: outer sensor output 51 mm apart from the joint center axis of the two parallel disks.

Above-mentioned observations can be also ascertained by the output of pressure sensors. The normalized pressure change measured by the digital oscilloscope is shown in figure 5. In this figure the pressure fluctuation for t*< 1.49 is also the noise caused by the electrical discharge. According to the output of digital stragescope, the first rebounds of the upper, middle and lower bubble and the second rebound of the upper bubble are detected in the lower wall sensor though these facts are illegible from figure 5. On the other hand, the rebounds of the lower and the middle bubble cannot be detected in the upper wall sensor. This is due to the presence of the upper bubble to

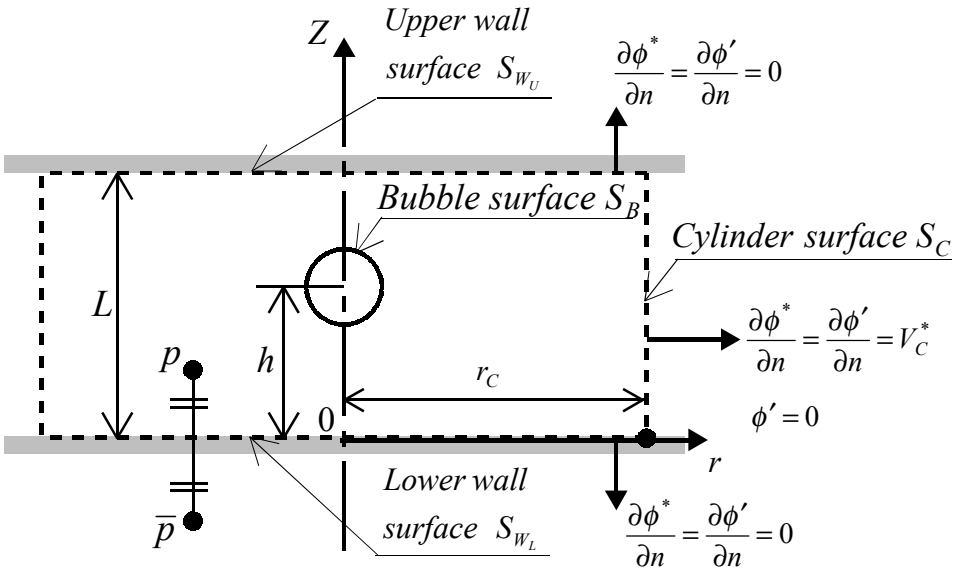

Figure 6: Computational domain and the boundary conditions

prevent the propagation of the shock wave. In this case the collapse phase shift among the divided bubbles brings the further damage on the lower wall surface.

3 Numerical Analysis

3.1 Computational Framework

In the present study numerical analyses were also performed to be compared with the above-mentioned bubble behavior. Assuming that the fluid is inviscid and incompressible and that the flow induced by the bubble's motion is irrotational, the velocity potential ϕ can be defined on the flow field. The coordinate definition is shown in figure 6. In the present computation it is also assumed that the flow field is axisymmetric with the joint center axis of the two parallel disks and that at the cylinder surface of $r=r_c$, ϕ and r-direction velocity component is uniform to the vertical direction and the pressure P is held constant of P_∞. Therefore we introduced a definite and two-dimensional computational domain shown in the figure as dashed line.

Moreover, if the effects due to buoyancy forces can be neglected, the normalized continuity equation and the equation of motion can be described as follows:

$$\nabla^2\phi^* = 0\,, \tag{2}$$

$$\frac{\partial\phi^*}{\partial t^*}+\frac{|\nabla\phi^*|^2}{2}+P^* = f(t^*)=\frac{\partial\phi_c{}^*}{\partial t^*}+\frac{V_c{}^*(t^*)^2}{2}\,, \tag{3}$$

where

$$P^* \equiv (P-P_\infty)/\Delta P\,,\quad V_c{}^* \equiv |\nabla\phi^*|_c = \left.\frac{\partial\phi^*}{\partial r}\right|_c\,, \tag{4}$$

and subscript c denotes the variables at the cylinder surface. When ϕ' is defined as $\phi' \equiv \phi^* - \phi_c{}^*(t^*)$, the equations (2) and (3) are also expressed as:

$$\nabla^2\phi' = 0\,, \tag{2}'$$

$$\frac{\partial\phi'}{\partial t^*}+\frac{|\nabla\phi'|^2}{2}+P^* = \frac{V_c{}^*(t^*)^2}{2}\,, \tag{3}'$$

and the boundary condition of ϕ' is described as shown in figure 6.

If we neglect the presence of non-condensable gas in the bubble, the equation of motion on the bubble surface can be described as follows:

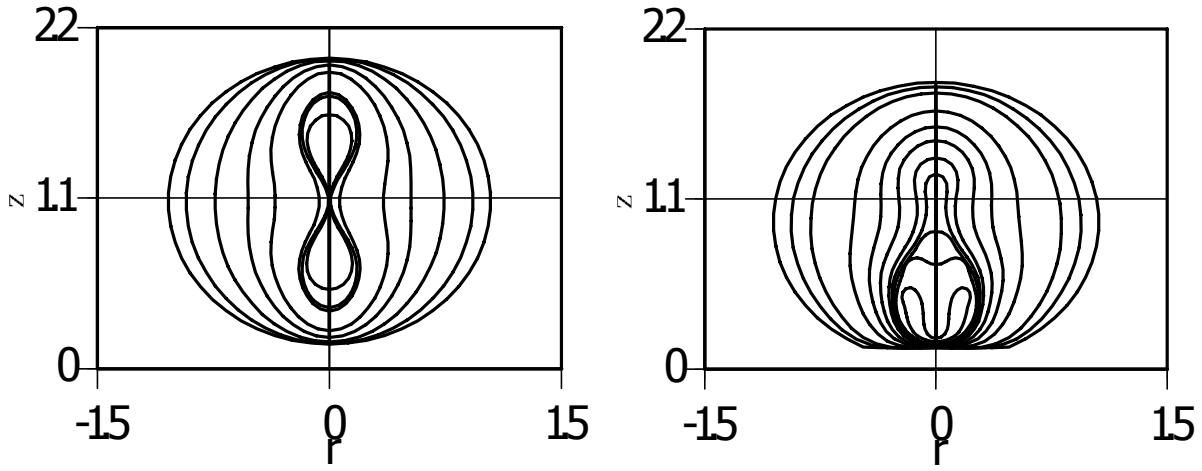

Figure 7: Computed bubble behavior between two parallel walls. Left: successive collapsing bubble shapes characterized by L^*=2.16, γ=1.08. The times corresponding to the profiles are t*=0 (outermost), 0.5359, 0.8293, 1.016, 1.115, 1.202, 1.208, 1.219 (innermost). Right: successive collapsing bubble shapes characterized by L^*=2.23, γ=0.95. The times corresponding to the profiles are t*=0 (outermost), 0.5356, 0.7507, 1.010, 1.105, 1.151, 1.180, 1.190, 1.195, 1.200, 1.212 (innermost).

$$\frac{D\phi'}{Dt^*} \equiv \frac{\partial \phi'}{\partial t^*} + |\nabla \phi'|^2 = \frac{|\nabla \phi'|^2}{2} + \frac{V_c^*(t^*)^2}{2} + 1 . \tag{5}$$

In the present study Laplace's equation (2)' was solved by the boundary element method (BEM). Considering the boundary conditions, the boundary-integral expression of (2)' becomes

$$C(\mathbf{p})\phi'(\mathbf{p}) = \int_{S_B} \left(G(\mathbf{p},\mathbf{x}) \frac{\partial \phi'}{\partial n}(\mathbf{x}) - \phi'(\mathbf{x}) \frac{\partial G}{\partial n}(\mathbf{p},\mathbf{x}) \right) ds(\mathbf{x}) - \int_{S_{W_U}} \phi'(\mathbf{x}) \frac{\partial G}{\partial n}(\mathbf{p},\mathbf{x}) ds(\mathbf{x}) + V_c^* \int_{S_c} G(\mathbf{p},\mathbf{x}) ds(\mathbf{x}) , \tag{6}$$

where

$$G(\mathbf{p},\mathbf{x}) = \frac{1}{4\pi}\left(\frac{1}{|\mathbf{x}-\mathbf{p}|} + \frac{1}{|\mathbf{x}-\bar{\mathbf{p}}|}\right), \quad V_c^* = \frac{1}{2\pi r_c^* L^*} \int_{S_B} -\frac{\partial \phi'}{\partial n} ds .$$

Herein $\mathbf{p}$ is the arbitrary point in the computational domain and $\bar{\mathbf{p}}$ is its image point in the plane z=0. Then C equals the solid angle when $\mathbf{p}$ is the boundary point, while it becomes unity when $\mathbf{p}$ is the interior point. As the problem is axisymmetric, equation (6) can be integrated in the azimuthal direction. The boundary of the computational domain was divided into several segments and the variables on the boundary were represented by the definite quantities defined at the nodes using appropriate interpolation methods. The numerical expression of (6) brings the simultaneous equations with respect to the unknown variables and they were numerically solved. After that the time integration on the equation (5) was performed using the second order Runge-Kutta method and these procedures were iterated.

In the present study the largest bubble shape, which is experimentally observed, was adopted as the initial shape and the following bubble collapse was computed. Moreover, the radius of the upper and lower disks 50 mm was used as the radius of the computational domain r_c.

3.2 Results and Discussion

Firstly, the bubble motion was computed for the case of L=15 mm and h=7.5 mm. In this case the normalized quantities L^*, γ and r_c^* becomes 2.16, 1.08 and 7.22, respectively. The results are shown in figure 7. The expanded bubble shrinks laterally and the narrow part is finally formed at the bubble center. In this process the vertical length is almost constant. These results are qualitatively in good agreement with the experimental ones. However afterwards the upper and lower bubble does not separate to the longitudinal direction but shrinks towards the bubble center. Moreover the total collapse time is very short when compared with the experimental one. In this study the presence of the non-condensable gas was neglected and, therefore, the effects of surrounding pressure were considered to be overestimated.

Secondly, the bubble motion corresponding to the case of L=15 mm and h=9 mm was computed. In this case the normalized quantities L^*, γ and r_c^* becomes 2.23, 0.95(=2.23-1.28) and 7.43, respectively. In this computation the initial bubble shape is turned upside down. In the present computation the effects due to buoyancy force was neglected and, therefore, this operation does not effect on the numerical results. The computed bubble motion is shown in figure 7. The lateral shrink makes the cone-shaped bubble and this also shows good agreement with the experimental observations. However the bubble does not separate to the vertical direction but shrinks towards the lower wall surface. Moreover the total collapse time is very short. These differences are also due to the effects of non-condensable gas.

4 Concluding Remarks

In the present study the bubble behavior in the narrow space are experimentally and numerically examined as the gap between two parallel walls and the position of bubble induction were changed. The main results are as follows:

(1) The effects of two parallel walls can be classified by the ratio of the gap between the walls to the maximum bubble radius. If the ratio>5.0 the bubble shape is almost sphere. The wall effect remarkably appears for the ratio<3.0 and the bubble deforms to be dumbbell- or cone-like shape.

(2) When the gap between the walls is small, the single bubble is finally divided into two bubbles owing to the large lateral pressure. The rebound of each bubble causes impulsive pressure and damages the upper and lower wall surface. Especially, if the bubble is not created at the center between the walls, the collapse phase shift among the divided bubbles brings the further damage on the wall surface.

(3) The computed motion of the bubble without non-condensable gases well explains the dumbbell- or cone-shaped bubble deformation. However the present computational model cannot explain the division of the single bubble into two bubbles. This remains our future works.

References

Best, J. P. and Kucera, A. 1992 A numerical investigation of non-spherical rebounding bubbles. *J. Fluid Mech.* **245**, 137-154.

Best, J. P. 1993 The formation of toroidal bubbles upon the collapse of transient cavities. *J. Fluid Mech.* **251**, 79-107.

Blake, J. R., Taib, B. B. and Doherty G. 1986 Transient cavities near boundaries. Part 1. Rigid boundary. *J. Fluid Mech.* **170**, 479-497.

Brennen, C. E. 1995 *Cavitation and bubble dynamics*. Oxford university press.

Chahine, G. L. 1982 Experimental and asymptotic study of nonspherical bubble collapse. *Appl. Sci. Res.* **38,** 187-197.

Kimoto, H. 1987 An experimental evaluation of the effects of a water microjet and a shock wave by a local pressure sensor. *Int. ASME Symp. on Cavitation Res. Facilities and Techniques.* **FED 57**, 217-224.

Kucherenko, V. V. and Shamko, V. V. 1986 Dynamics of electric-explosion cavities between two solid parallel walls. *J. Appl. Mech. Tech. Phys.* **27**, 112-115.

Lauterborn, W. and Bolle, H. 1975 Experimental investigations of cavitation-bubble collapse in the neighborhood of a solid boundary. *J. Fluid Mech.* **72**, 391-399.

Plesset, M. S. and Chapman R. B. 1971 Collapse of an initially spherical vapour cavity in the neighborhood of a solid boundary. *J. Fluid Mech.* 47, 283-290.

Shima, A. and Sato, Y. 1981 The bubble behavior in the narrow space. *Rep. Inst. High Speed Mech. Tohoku Univ.* **47**, 61-77. (in Japanese)

Takahira, H., Sakai, N. and Akamatsu T. 1997 Numerical analysis of toroidal bubbles by the boundary element method (Effects of bubble-bubble/bubble-wall interactions). *Trans. JSME* B **63**, 1496-1504. (in Japanese)

Tomita, Y. and Shima, A. 1990 High-speed photographic observations of laser-induced cavitation bubbles in water. *Acustica* **71**, 161-171.